ALGORITHM THEORETICAL BASIS DOCUMENT (ATBD):

LEAF AREA INDEX

PREPARED BY	ORGANIZATION	DATE
David Hulslander	AOP	05/29/2019

APPROVALS	ORGANIZATION	APPROVAL DATE
David Barlow	SYS	6/11/2019

RELEASED BY	ORGANIZATION	RELEASE DATE
Anne Balsley	CM	07/01/2019

See configuration management system for approval history.

Change Record

REVISION	DATE	ECO #	DESCRIPTION OF CHANGE
A	07/01/2019	ECO-06170	Initial Release

TABLE OF CONTENTS

LIST OF TABLES AND FIGURES

Figure 1 Portions of the electromagnetic spectrum showing % atmospheric transmission and the bandpasses for Landsat 7 (ETM+) and Landsat 8 (OLI and TIRS) sensors. Landsat 8 OLI Bands 2, 3, 4, and 5

1   DESCRIPTION

Contained in this document are details concerning Airborne Observation Platform (AOP) Leaf Area Index (LAI) measurements made at all NEON sites. Specifically, the processes necessary to convert "raw" sensor measurements into meaningful scientific units and their associated uncertainties are described. Neon Imaging Spectrometer (NIS) data collection is planned for each NEON site annually at 90% maximum greenness or greater.

1.1 Purpose

This document details the algorithms used for creating NEON Level 2 data product Leaf Area Index (LAI) for NEON Imaging Spectrometer (NIS) from Level 1 data, and ancillary data as defined in this document (such as calibration data) obtained via instrumental measurements made by the NIS. It includes a detailed discussion of measurement theory and implementation, appropriate theoretical background, data product provenance, quality assurance and control methods used, approximations and/or assumptions made, and a detailed exposition of uncertainty resulting in a cumulative reported uncertainty for this product.

1.2 Scope

The theoretical background and entire algorithmic process used to derive NEON Level 2 data product Leaf Area Index (LAI) from Level 1 data for NIS is described in this document. The NIS employed is the NEON Imaging Spectrometer (NIS), JPL AVIRS NextGen Imaging Spectrometer. This document does not provide computational implementation details, except for cases where these stem directly from algorithmic choices explained here.

2   RELATED DOCUMENTS, ACRONYMS AND VARIABLE NOMENCLATURE

2.1 Applicable Documents

AD[01]	NEON.DOC.000001	NEON OBSERVATORY DESIGN
AD[02]	NEON.DOC.002652	NEON Level 1, Level 2 and Level 3 Data Products Catalog
AD[03]	NEON.DOC.000782	ATBD QA/QC Data Consistency
AD[04]	NEON.DOC.011081	ATBD QA/QC Plausibility Tests
AD[05]	NEON.DOC.000783	ATBD De-spiking and Time Series Analyses
AD[06]	NEON.DOC.000746	Calibration Fixture and Sensor Uncertainty Analysis (CVAL)
AD[07]	NEON.DOC.000785	TIS Level 1 Data Products Uncertainty Budget Estimation Plan
AD[08]	NEON.DOC.000927	NEON Calibration and Sensor Uncertainty Values
AD[09]	NEON.DOC.001113	Quality Flags and Quality Metrics for TIS Data Products

2.2 Reference Documents

RD[01]	NEON.DOC.000008	NEON Acronym List
RD[02]	NEON.DOC.000243	NEON Glossary of Terms
RD[03]	NEON.DOC.001288	NEON Imaging spectrometer radiance to reflectance algorithm theoretical basis document
RD[04]	NEON.DOC.001290	NEON Algorithm Theoretical Basis Document: Imaging Spectrometer Geolocation Processing
RD[05]	NEON.DOC.001210	NEON Algorithm Theoretical Basis Document: NEON Imaging Spectrometer Level 1B Calibrated Radiance

2.3 Acronyms

Acronym	Explanation
AIS	Aquatic Instrument System
ATBD	Algorithm Theoretical Basis Document
CI	NEON Cyberinfrastructure
CVAL	NEON Calibration, Validation, and Audit Laboratory
DAS	Data Acquisition System
DP	Data Product
FDAS	Field Data Acquisition System
GRAPE	Grouped Remote Analog Peripheral Equipment
Hz	Hertz
L0	Level 0
L1	Level 1
PRT	Platinum resistance thermometer
QA/QC	Quality assurance and quality control

3   DATA PRODUCT DESCRIPTION

3.1 Variables Reported

The NIS-related L1 DPs provided by the algorithms documented in this ATBD are available via NEON AOP Data Request.

3.2 Input Dependencies

Table 1 - List of NIS-related DPs that are transformed into L1 NIS DPs in this ATBD.

Description	Sample Frequency	Units	Data Product Number
Directional Surface Reflectance	**Yearly**	**%**	**NEON.DOM.SITE.DP1.30006.001**

3.3 Product Instances

The NEON Imaging Spectrometer (NIS) will be deployed at all NEON terrestrial sites and most NEON aquatic sites.

3.4 Temporal Resolution and Extent

Current NEON AOP plans have airborne surveys for sites to be completed annually at 90% or higher of maximum greenness for the lifetime of the Observatory.

3.5 Spatial Resolution and Extent

All sites surveyed contain the airshed(s) for NEON towers and a minimum of 10 km x 10 km surrounding that. Survey areas may be larger than the minimum if adjacent towers create overlapping survey areas, if watersheds extend from the minimum area in an easily surveyed configuration, or if other conditions create targets of opportunity for high value data at minimal or no cost. LAI is based entirely on NEON Imaging Spectrometer (NIS) reflectance data, which is published as 1 m pixels. Hence, LAI data are produced with 1 m pixels.
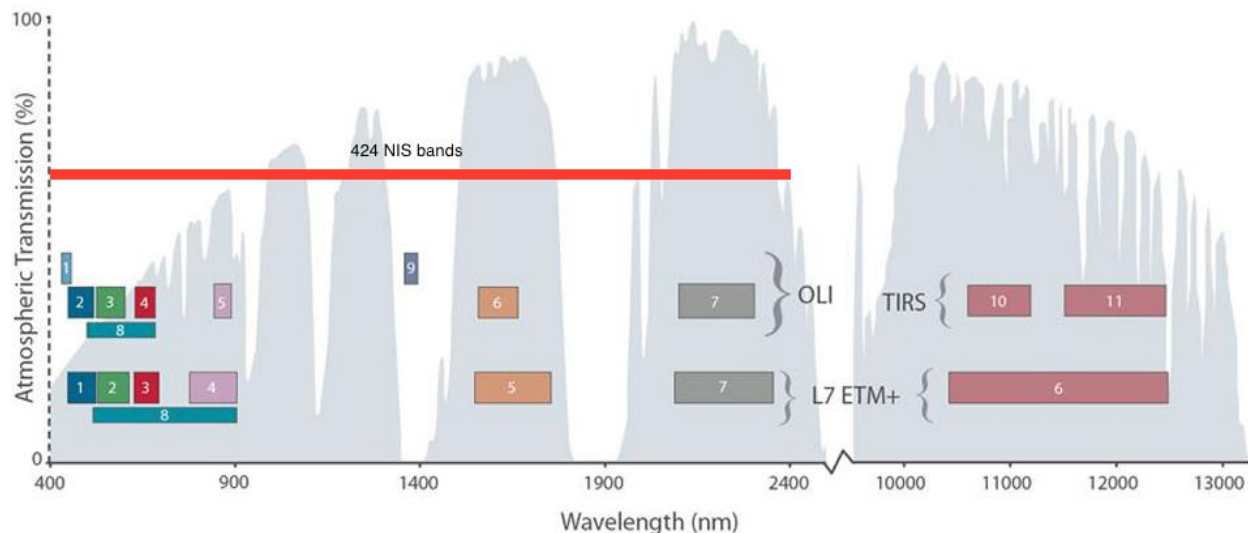
4   SCIENTIFIC CONTEXT

NEON's Airborne Observation Platform (AOP) remote sensing payload includes the NEON Imaging Spectrometer (NIS), a visible-to-shortwave infrared (VSWIR) pushbroom sensor; a small-footprint full waveform LiDAR, and a high-resolution digital camera. The instrument payload is mounted onto a common integration plate, the Platform Integration Mount, or PIM . The entire AOP remote sensing payload is integrated onto a de Havilland DHC-6 Twin Otter aircraft configured with a large open downward-looking viewport. The payload is mounted directly on the cabin floor via the seat rails with the sensors viewing in the nadir direction through an open port. Imaging spectrometer data acquired with the NIS instrument supports the creation of derived data products which give unique insight into the types, abundance, and quality of various land covers, including vegetation (Govender, Chetty, & Bulcock, 2007).

4.1 Theory of Measurement

Level 1 NIS reflectance data provide atmospherically adjusted at-ground reflectance spectra for each pixel in 424 discrete 5 nm bandpasses for wavelengths from 382 nm to 2512 nm (RD[05]). The unique reflectance spectra of materials on the ground are captured in this data. As full spectral curves are difficult and cumbersome to process and analyze, applications typically utilize only those spectral regions relevant to the materials or phenomena of interest and their key spectral features. This approach also works well with the much broader bandpasses of multispectral sensors. For vegetation, these spectral features and regions include blue reflectance, the green vegetation reflectance feature and its shoulders, the chlorophyll absorption feature in the red wavelengths, the near infrared (NIR) shoulder, and the lignin reflectance feature in the shortwave infrared (SWIR). The regions are shown in **Figure 1** in the larger context of the electromagnetic spectrum as well as how they relate to the commonly used Landsat 7 and 8 bandpasses.

Figure 1 Portions of the electromagnetic spectrum showing % atmospheric transmission and the bandpasses for Landsat 7 (ETM+) and Landsat 8 (OLI and TIRS) sensors. Landsat 8 OLI Bands 2, 3, 4, and 5 correspond to Blue, Green, Red and Near Infrared (NIR), respectively. Landsat has used 4 to 9 bands, depending on generation, to cover the roughly 400 to 2400 nm portion of the spectrum here, which is covered by the NEON Imaging Spectrometer with 424 5-nm-wide bands. ("Landsat 8 « Landsat Science," n.d.)

For spectral indices, the reflectance values of those regions are combined using various functions, typically as normalized ratios of two or more bands. This reduces the data volume to a single value per pixel directly related to the topic of study and comparable across both space and time and even between different sensors and datasets. Using ratios can also help reduce error, as it is inherently a relative measure and eliminates error common to the absolute measure of the bands involved. Many such indices are now common in remote sensing and the earth sciences (Miura, Tsend-Ayush, & Turner, n.d.).

Numerous links and correlations between these indices and biophysical parameters have been found (Huete et al., 2002). One parameter of particular interest is green Leaf Area Index (LAI). It is used in many different fields in earth science for understanding and predicting processes and change in vegetated land covers. LAI is a unitless ratio computed by dividing the area of ground in to the total area of foliage above it. For example, a 4-meter square pixel with an LAI value of 1.8 should have 7.2 square meters of green leaves or needles above it, as shown in **Eq. 1**.

$$LAI = \frac{A_{leaf}}{A_{ground}} = \frac{7.2\ m^2}{1.8\ m^2} = 1.8$$

<div align="right">**Eq. 1**</div>

Physically measuring LAI in the field, while often very accurate, is difficult, expensive, and cannot be scaled to gain full coverage at the landscape, regional, and global scales. Airborne and satellite remote sensing methods of measuring LAI can cover the larger scales at reasonable cost efficiencies but are based on spectral measurements and algorithms such as indices and as a result are proxy measurements rather than direct biophysical measurements.

4.2 Theory of Algorithm

Two main drawbacks have been found when using remotely sensed spectral indices to predict and compute LAI :

1. Regions with LAI values in the range of 2 to 5 rapidly saturate common vegetation indices.
2. There is no unique relationship between LAI and any particular vegetation index yet developed.

The relationship of LAI to any particular vegetation index is influenced by a multivariate and interdependent set of factors including but not limited to:

- Bidirectional reflectance distribution function (BRDF) of the ground cover
- Sensor data acquisition geometry

- Solar elevation angle and illumination geometry
- Chlorophyll content
- Canopy structure

While there has been continuous work on developing vegetation indices which better allow for deriving LAI from remotely sensed data, a perfect and robust solution does not yet exist, particularly for use across a broad variety of ground covers and geography. The NEON LAI remote sensing data product uses the best currently available compromise with the most widely used algorithm and implementation, the ATCOR LAI equation based on Soil-Adjusted Vegetation Index (SAVI) as seen in **Eq. 2**.

$$SAVI = \frac{(\rho_{850} - \rho_{650}) * 1.5}{\rho_{850} + \rho_{650} + 0.5}$$

Eq. 2

5 ALGORITHM IMPLEMENTATION

Data flow for processing of AOP L1 NIS to produce L2 and L3 LAI data products will be performed in the following manner.

1. L1 NIS Surface Directional Reflectance (reference here) will be processed through the AOP data processing pipeline for producing L2 Vegetation Index data products (reference here).
2. The AOP data processing pipeline will then access the Soil-Adjusted Vegetation Index (SAVI) portion of the L2 vegetation index products as input to the LAI algorithm as seen in **Eq. 3**.

$$LAI = \frac{-1}{0.60} ln\left(\frac{0.82 - SAVI}{0.78}\right)$$

Eq. 3

3. The AOP data processing pipeline will write the LAI results of step 2 out to GeoTIFF files, one for each flight line.
4. The AOP data processing pipeline will use all L2 LAI files for a given site to produce a Level 3 geospatial mosaic product optimizing pixel data value assignment using rules implemented to best mitigate error from cloud cover, illumination geometry, and acquisition geometry.
5. The AOP data processing pipeline will write the results of step 4 out to L3 LAI data product GeoTIFF files using a regular grid (reference to LiDAR grid here).

QA/QC Procedure:

QA/QC procedures for the LAI data product will include both manual and programmatic approaches as described below:

1. **Plausibility Tests** The plausibility of a given pixel's LAI value depends on both the value itself and the type of ground cover. For example, an LAI value greater than 10 may be quite reasonable for

a dense conifer forest, but is completely implausible in a grassy area or corn field. NEON LAI products will be manually spot checked for implausible values. As ground data from field observations becomes available, they will be incorporated in to automated QA/QC procedures. As the links between the ground cover, LiDAR data, and NIS data become better understood in the initial years of the Observatory, more discerning automated processing and QA/QC steps will be added.

2. **Sensor Flags** Because LAI is a derived product, produced from an upstream derived product (SAVI) based entirely on NIS data, the final LAI product will only have sensor flags as generated for NIS data.

3. **Quality Flags (QFs) and Quality Metrics (QMs)** Manual QA/QC will be performed where uncertainty values are high and/or where data quality or sensor flags indicate potential issues. Checking these areas against imagery will indicate if they are anomalous but acceptable (e.g. unusual land cover) or if there is a data or processing problem.

6   UNCERTAINTY

Because the Leaf Area Index product as described in this document is entirely derived from L1 NIS surface reflectance data combined in a normalized ratio (SAVI), its uncertainty is therefore entirely dependent on the uncertainty in the L1 reflectance data and the combinations and ratios of bands used in SAVI. Additional sources of errors or uncertainties will be included in analysis as they are identified during the course of observatory construction and operation. There are a number of sources of uncertainty contributing to the reflectance data product uncertainty, as shown in **Figure 2**. The detailed analysis of uncertainty in the reflectance data is discussed in the L1 Reflectance ATBD. The reported uncertainty values from the L1 Reflectance ATBD are used here. A summary of them is in

Table 2.

Table 2 Summary of expected reflectance uncertainties due to site and observing conditions, data acquisition procedures, instrumentation nature, and data processing requirements.

| Data Quality	Surface Type	Atmospheric Conditions	ρ Error (% reflectance)
Ideal	Well characterized, low complexity	Well characterized, spatially and temporally consistent, clear	± 2%
Medium	Moderately complex, moderately well characterized	Some spatial and temporal variation, moderate haze and aerosol	± 5%
Low	Highly complex and/or poorly characterized	Poorly characterized, highly variable, anomalous conditions	± 10%
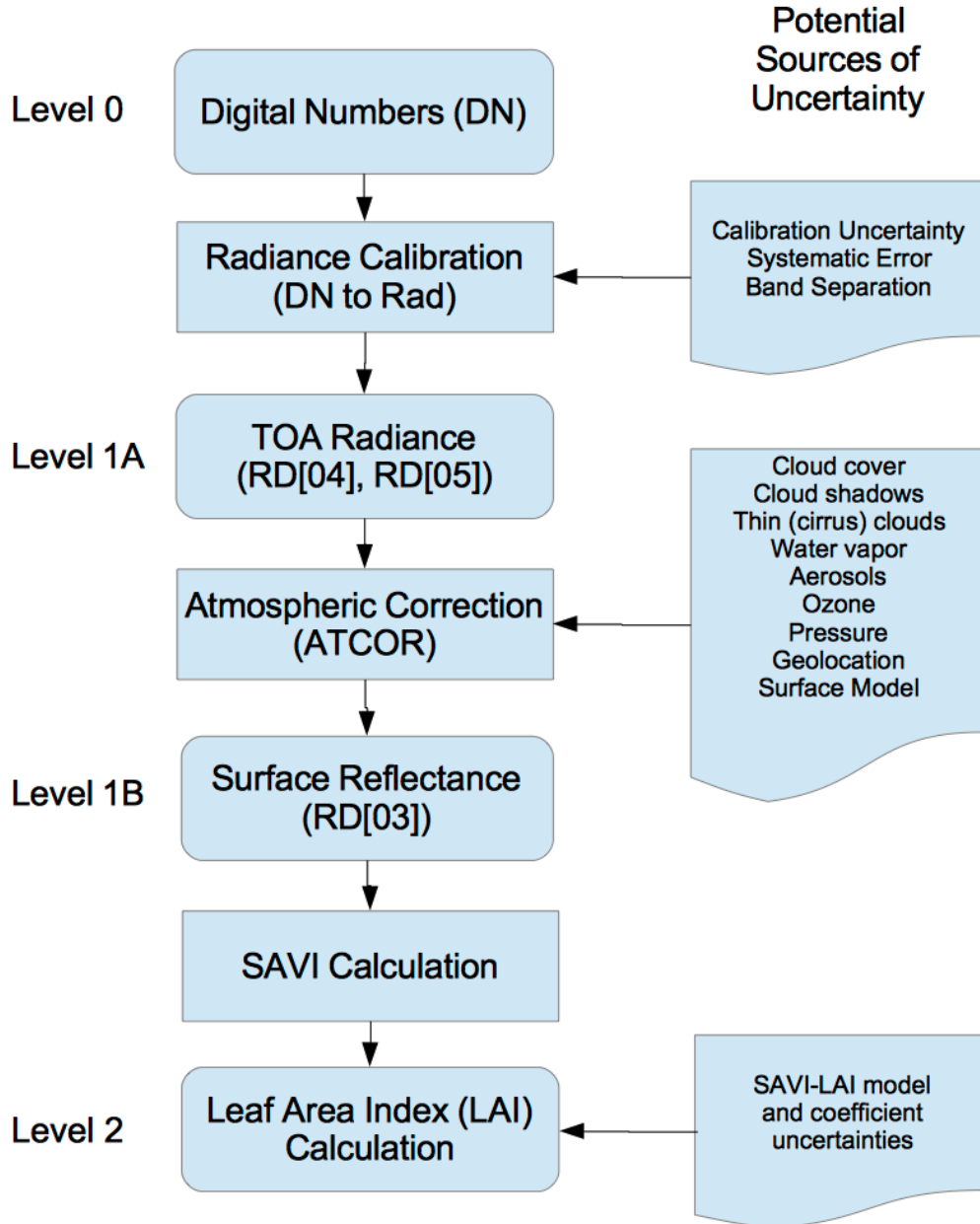
Figure 2 End-to-end analysis of vegetation index uncertainty including sources of uncertainty in upstream processing and systems contributing to the reflectance data input required for calculating vegetation indices.

6.1 Analysis of Uncertainty

Propagation and accumulation of uncertainty from sources in to the Leaf Area Index can be modeled using the "law of propagation of uncertainty" (NCSL, 1997, Taylor and Kuyatt, 1994). This approach handles only random errors, does not consider systematic biases, and assumes statistical independence in the errors. Systematic errors and biases are addressed in the processing of the raw NIS data to the surface reflectance values used here (RD[03], RD[04], RD[05]). As has been done with MODIS vegetation indices, we use the framework of vegetation indices being a quantity of interest y based on a function combining estimates of n other quantities as shown in **Eq. 4** (Huete, Justice, & Van Leeuwen, 1999).

$$y = f(x_1, x_2, \ldots, x_n)$$

<div align="right">**Eq. 4**</div>

An uncertainty propagation equation, **Eq. 5**, can be based on a first-order Taylor series expansion of **Eq. 4**, where u is uncertainty (Huete et al., 1999).

$$u^2 = \sum_{i=1}^{n}\sum_{j=1}^{n} \frac{\partial f}{\partial x_i}\frac{\partial f}{\partial x_j} u(x_i, x_j) = \sum_{i=1}^{n}\left(\frac{\partial f}{\partial x_i}\right)^2 u^2(x_i) + 2\sum_{i=1}^{n-1}\sum_{j=i+1}^{n} \frac{\partial f}{\partial x_i}\frac{\partial f}{\partial x_j} u(x_i, x_j)$$

<div align="right">**Eq. 5**</div>

From **Eq. 5** a set of uncertainty propagation equations designed for reflectance calibration uncertainties in atmospherically corrected vegetation indices can be created, as are shown in their respective sections in the Vegetation Index ATBD. From the uncertainty equation for SAVI, an equation for error in LAI can be derived, as shown in **Eq. 6**.

$$\frac{\partial LAI}{\partial SAVI} = \frac{1}{a_2(a_0 - SAVI)}$$

<div align="right">**Eq. 6**</div>

From the above equations, it can be seen that the error in LAI will vary with both the error of the input reflectance and with the actual reflectance values. Error in LAI has been calculated for all combinations of ρ_{650} and ρ_{850} reflectance values from 5% to 75% for 2%, 5%, and 10% error in those values. It is important to note that LAI calculated this way becomes undefined as the calculated SAVI value

approaches 0.82, the value for the constant a_0. The surface plots for the error in LAI for 2%, 5%, and 10% reflectance are in **Figure 3**, **Figure 4**, and **Figure 5**, respectively.
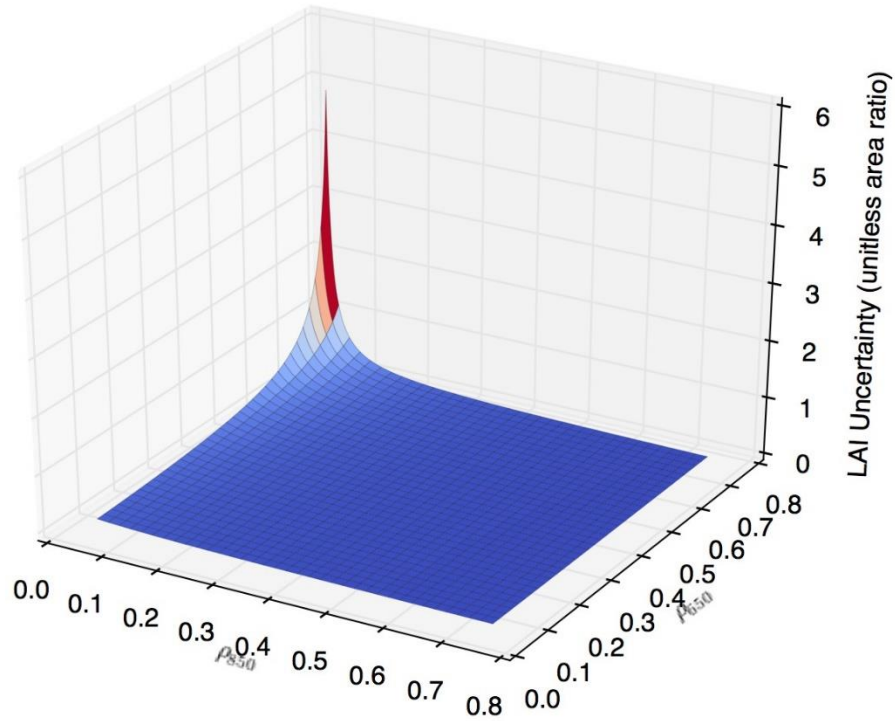

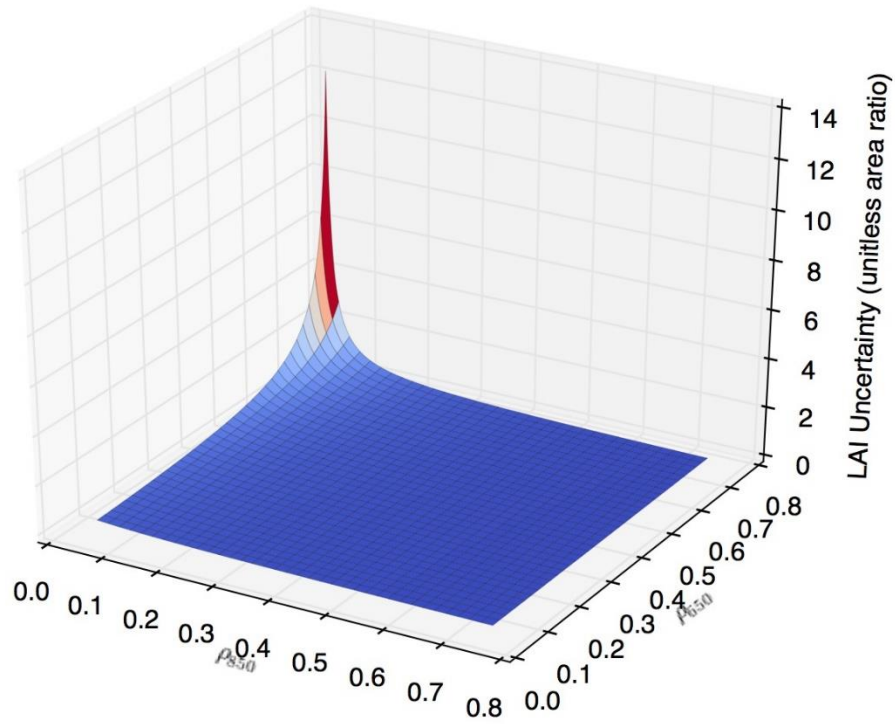**Figure 3 Error in LAI as a function of input reflectance values with 2% uncertainty.**

Figure 4 Error in LAI as a function of input reflectance values with 5% uncertainty.
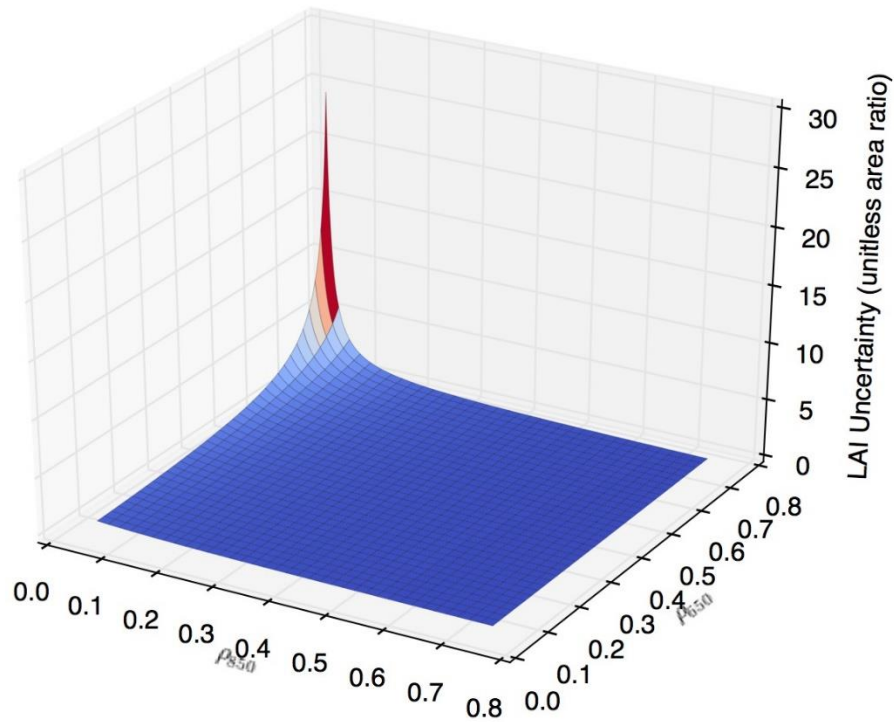
Figure 5 Error in LAI as a function of input reflectance values with 10% uncertainty.

7   FUTURE PLANS AND MODIFICATIONS

Plans for future improvements and upgrades to the NEON LAI data product include:

- Using NEON ground-based LAI measurements to adjust model coefficients.
- Developing and using ways to use the co-collected LiDAR data (discrete and/or waveform) to adjust model coefficients across areas or on a per-pixel basis, or even to develop a new and improved model for calculating LAI from the spectrometer and LiDAR data.
- Possibly including land cover information from co-collected imagery or other sources on an area or per pixel basis for coefficient adjustment or intelligent model selection.

8   BIBLIOGRAPHY

Govender, M., Chetty, K., & Bulcock, H. (2007). A review of hyperspectral remote sensing and its application in vegetation and water resource studies. *Water Sa*, *33*(2). Retrieved from http://www.ajol.info/index.php/wsa/article/view/49049

Huete, A., Didan, K., Miura, T., Rodriguez, E. P., Gao, X., & Ferreira, L. G. (2002). Overview of the radiometric and biophysical performance of the MODIS vegetation indices. *Remote Sensing of Environment*, *83*(1), 195–213.

Huete, A., Justice, C., & Van Leeuwen, W. (1999). MODIS vegetation index (MOD13). *Algorithm Theoretical Basis Document*, *3*, 213.

Landsat 8 « Landsat Science. (n.d.). Retrieved from http://landsat.gsfc.nasa.gov/landsat-data-continuity-mission/

Miura, T., Tsend-Ayush, J., & Turner, J. P. (n.d.). Compatibility Analysis of Multi-Sensor Vegetation Indices Using EO-1 Hyperion Data. Retrieved from http://www.isprs.org/proceedings/2011/isrse-34/211104015Final00571.pdf